Single-crystal studies of incommensurate Na to 1.5 Mbar

Single-crystal studies of incommensurate Na to 1.5 Mbar

L. F. Lundegaard, E. Gregoryanz, M. I. McMahon, C. Guillaume, I. Loa, and R. J. Nelmes
SUPA, School of Physics and Astronomy, and Centre for Science at Extreme Conditions, The University of Edinburgh, Mayfield Road, Edinburgh EH9 3JZ, United Kingdom

(Received 4 September 2008; published 9 February 2009)

Synchrotron single-crystal diffraction data show that sodium transforms from the oP8 structure to an incommensurate host-guest composite structure above 125 GPa in which the guest component is nearly "melted." At 147 GPa, the correlation length between the guest chains is only 28(3) Å, or approximately six times the chain spacing. This configuration shows a wide range of stability from above 125 GPa to at least 155 GPa and 550 K. The transition to this phase is accompanied by a marked decrease in optical reflectivity. Electronic band-structure calculations are used to interpret this change.

DOI: 10.1103/PhysRevB.79.064105 PACS number(s): 61.50.Ks, 62.50.−p

Among the metallic elements, the alkali metals occupy a special place due to the simplicity of their electronic structure. Because they are nearly free-electron (NFE) metals at ambient conditions and their Fermi surfaces are nearly spherical, they have been, and remain, a fertile testing ground for theory and experiment alike (see Refs. 1–3, and references therein). The simple approach of ignoring the ionic core structure by replacing it with a uniform positively charged background (the so-called jellium model) led to significant insights into the electronic band structure of solids. However, this approximation does not hold at higher densities, where the NFE metals depart from free-electron-like behavior, and exhibit a wide spectrum of pressure-induced phenomena ranging from the adoption of low-symmetry structures[4–6] to the onset of superconductivity[7–9] and very unusual behavior of the melting curve in the case of Na.[10] Most recently, a study of highly compressed Na in the vicinity of its melting minimum at 118 GPa and 300 K has revealed the existence of numerous well crystallized and very complex solid phases.[11] The number of phases and the narrow range of pressures and temperatures over which they exist suggest a very flat free-energy surface with several local minima.[11] This and the unique melting curve behavior create considerable interest in understanding the liquid and solid structures in this region, including possible relationships to the predicted behavior of hydrogen.[11]

Sodium at 295 K has a body-centered-cubic structure at ambient pressure, which transforms to a face-centered-cubic structure at 65 GPa, and then to a more complex 16-atom body-centered-cubic (cI16) structure at 105 GPa.[12,13] (cI16 is a standard notation[14] designating the lattice symmetry and the number of atoms in the unit cell.) Single-crystal diffraction data have been used to refine the full structures of cI16,[13] and of the orthorhombic oP8 phase observed at 295 K between 118 and 125 GPa.[11,12] At 125 GPa, there is a transition to a phase with a diffraction pattern containing sharp Bragg reflections and much weaker layers of diffuse scattering,[11] which can be interpreted in terms of a host-guest composite incommensurate structure as previously found in a number of elemental metals.[15] This structure is designated as tI19. The data revealed four other, previously unknown, complex phases occurring between 295 K and the melting line, close to its minimum, with tetragonal, orthorhombic, monoclinic, and triclinic symmetries, and with approximately 52, 120, 512, and 90 atoms, respectively, per unit cell.[11] The full structures of these and of the tI19 phase remain to be determined.

In this paper, we report single-crystal diffraction studies of tI19 to 155 GPa, and a detailed structure determination at 147 GPa. This is the highest pressure at which full crystal-structure refinements by single-crystal methods have been carried out, and extends such studies well into the 100–200 GPa range. We show that the host component is isostructural with that observed previously in the alkali metals Rb and K.[6,16] However, the arrangement of the one-dimensional (1D) guest chains within the host framework is different from those observed previously in Rb-IV and K-III. Moreover, the broadened nature of the guest Bragg reflections reveals that the guest chains are partially disordered over the whole pressure range studied, with an interchain correlation length of ~30 Å at 147 GPa. We also observed abrupt darkening of the sample at 125 GPa upon entering the incommensurate phase.

Single-crystal diffraction data were collected on beamline ID27 at the European Synchrotron Radiation Facility using an x-ray wavelength of 0.3738 Å and a beam size of 6×6 μm^2 full width at half maximum (FWHM). The distance from the sample to the area detector and the detector tilts were determined with a LaB_6 standard. Sodium with a stated purity of 99.95% was loaded without a pressure-transmitting medium into the diamond-anvil cell in a dry argon atmosphere to prevent oxidation of the sample. The pressure cell was equipped with Boehler-Almax-type seats and beveled diamond anvils,[17] which provided a conical aperture (full angle) of 52°. A few grains of polycrystalline tantalum (grain size of 2–3 μm) were enclosed with the sodium for pressure measurement. Pressures were derived from the published Na equation of state up to the cI16 phase[3] and, above that, the relative pressures were obtained from the Ta calibrant.[18] Diffraction patterns of the low-pressure sodium phases showed no discernible contaminant peaks, confirming that the samples were pure. The diffraction data were collected on either a charge-coupled device (CCD) or an image-plate detector in a sequence of contiguous 0.25° oscillations over a total scan range of $\omega=50°$ around the vertical axis. After rotating the pressure cell 90° around the incident x-ray beam, a second ω scan of 50° was made. The intensities of the Bragg reflections were integrated by using

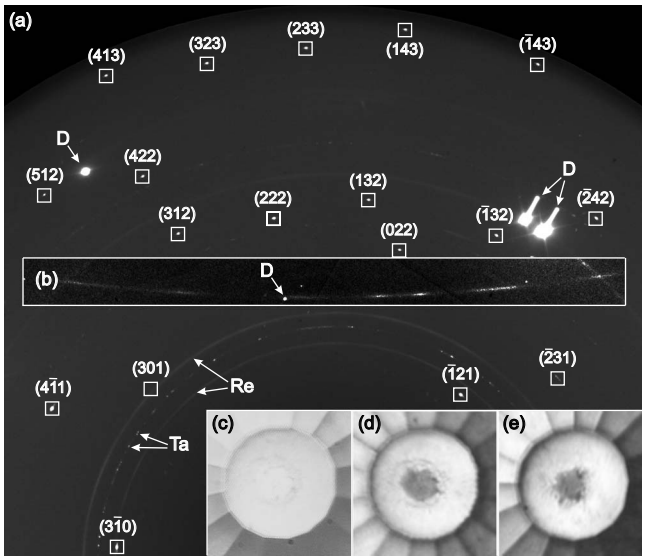

FIG. 1. (a) Approximately half a diffraction image from the tI19 phase of Na at 130 GPa, obtained in a ±10° oscillation. Eighteen observed host reflections are marked and indexed. As labeled, the smooth powder-diffraction rings in the lower part are from the rhenium gasket and the spotty ring is from the tantalum pressure marker. Reflections marked with "D" are from the diamond anvils. A section, (b), has been replaced with a long-exposure nonoscillated diffraction image collected in the same orientation and with its contrast enhanced to reveal the first layer of very weak reflections from the guest component. The lower-right insets show (c) a sample at 122 GPa in the oP8 phase, (d) the same sample at 127 GPa in the tI19 phase, and (e) a second sample at 155 GPa in the tI19 phase, all as viewed in reflected white light. The sample is not distinguishable from the gasket in (c) but has the same size and shape as in (d).

the SAINT program[19] and the structure was refined on intensities using SHELXL97.[20]

Single-crystal samples of incommensurate Na were grown in two different pressure cells by slow pressure increase from single crystals of the oP8 phase, which were themselves grown from the melt at 118 GPa.[11] The phase transition from the oP8 phase was observed at 125(2) GPa, and the quality of the crystals of the higher pressure phase was excellent, with sharp Bragg reflections from the host component of the structure (the full peak width at half maximum of the rocking curve was less than 0.4°). There were also layers of diffuse scattering which contained much broadened Bragg reflections from the guest component. The much different appearances of the host and guest reflections are illustrated in Fig. 1, which shows a composite diffraction image from Na at 130 GPa. The transition from the oP8 phase was accompanied by a marked reduction in the reflectivity of the sample, as illustrated in Fig. 1. The inset (c) of Fig. 1 shows an oP8 sample with a reflectivity close to that of the surrounding rhenium gasket, and inset (d) shows the same sample in the tI19 phase reflecting much less than the rhenium. The absence of any change in the apparent reflectivity of the gasket material surrounding the sample when passing into the tI19 phase suggests that the observed change in reflectivity of the sample does not arise from any effect within the diamond anvils. The inset (e) indicates that the reflectivity remains approximately the same at 155 GPa.

The positions of the *host* reflections at 130 GPa could all be accounted for by a body-centered tetragonal lattice with lattice parameters $a_{\text{host}}=7.0880(7)$ Å and $c_{\text{host}}=3.4810(3)$ Å, and the systematically absent reflections were consistent with space-group $I4/mcm$. The host is isostructural with that observed in the composite structures of the alkali metals K and Rb.[6,16] The guest reflections determine the c_{guest} lattice parameter of 2.12(1) Å, and the $c_{\text{host}}/c_{\text{guest}}$ ratio is then 1.64(1). The estimated volume decrease at the oP8 to tI19 transition is 0.5(2)%. Integration of the host Bragg reflections yielded 116 reflections that did not saturate the detector, which were averaged over symmetry equivalents to yield 20 independent host-only reflections, that is, (hkl) with $l\neq 0$, of which 19 had $I>4\sigma(I)$. The internal consistency was $R_{\text{sym}}=7.4\%$. Refinement of these 19 host-only reflections in space-group $I4/mcm$ with atoms on the 16*k* Wykoff site at $(x,y,\frac{1}{2})$ gave refined atomic coordinates of $x=0.7899(2)$ and $y=0.0882(2)$, and an isotropic atomic displacement parameter for the host atoms of $U_{\text{iso}}=0.018(2)$ Å^2. The fit to the data was excellent, with an *R* factor of 2.9% and a goodness of fit (χ^2) of 0.98.

The weakness of the guest reflections at 130 GPa and their broadness made their analysis difficult. Similarly broad guest reflections were observed previously in Rb-IV between 16.2 and 16.7 GPa but were found to sharpen on pressure increase above 16.7 GPa.[21] We therefore increased the pressure on the Na sample to investigate whether the same phenomenon would be observed. However, up to 155 GPa, the highest pressure reached in this study, the guest reflections remained broad with no observable change in their width.

Full data were collected at 147 GPa. The large intensity difference between the Bragg reflections from the host and guest components meant that *two* separate data collections were needed to obtain full structural information. The first, optimized for the strongly scattering host component, yielded 185 individual host-only reflections, which were averaged to yield 34 independent reflections, all with $I>4\sigma(I)$, with an internal consistency of $R_{\text{sym}}=6.0\%$. (The greater number of reflections at 147 GPa is a result of ensuring that fewer reflections saturated the detector than at 130 GPa.) The refined lattice parameters were $a_{\text{host}}=6.996(2)$ Å and $c_{\text{host}}=3.399(2)$ Å, and the refined coordinates of the host atoms were $[0.7898(2),0.0880(2),\frac{1}{2}]$, the same within error as those observed at 130 GPa. The refined value of the isotropic atomic displacement parameter of the host atoms was $U_{\text{iso}}=0.012(1)$ Å^2. The fit to the data was again excellent with an *R* factor of 2.9% and a goodness of fit of 1.09.

A second data collection at 147 GPa was optimized for the guest component with exposures ~130 times longer than the first. This resulted in saturation of all the host reflections but it was possible to index each of the (still very weak) guest peaks using the orientation matrix of the host component obtained in the first data collection. Only two layers of guest reflections $(hk\pm 1)$ were observed and they yielded a 2.05(1) Å separation of guest atoms along the *c* axis, which corresponds to a $c_{\text{host}}/c_{\text{guest}}$ ratio of 1.66(1), the same as the maximum value reached in Rb-IV.[16] The ratio is thus almost constant with pressure unlike in K-III (Ref. 6) and Rb-IV.[16] However, the arrangement of the guest-atom chains is quite different from that in Rb-IV (and from that in K-III). The

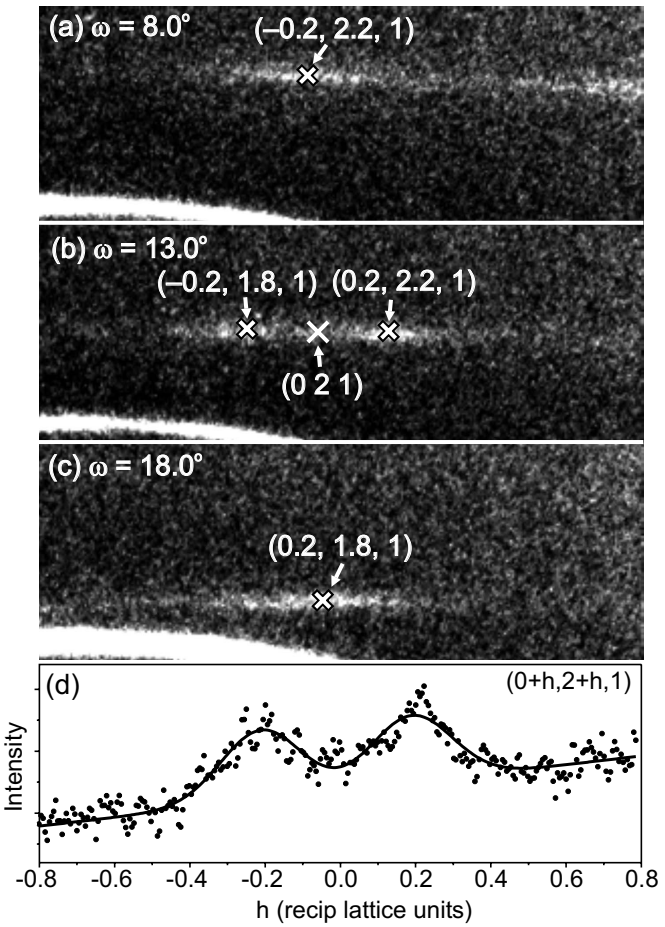

FIG. 2. Parts of a sequence of diffraction patterns from tI19-Na at 147 GPa enlarged to show four broadened guest reflections that appear as a function of the cell rotation angle ω. They are displaced equally about the calculated (021) position (marked with a cross) for a tetragonal unit cell with $a_{\text{guest}}^{\text{tetrag}}=7$ Å and $c_{\text{guest}}=2.05$ Å, and index as (–0.2,2.2,1), (–0.2,1.8,1), (0.2,2.2,1), and (0.2,1.8,1). Panel (d) shows an integrated profile through the two guest reflections in panel (b), along with a two-Gaussian fit (solid line).

guest reflections in Na comprise groups of four reflections displaced symmetrically about the $(hk\pm1)$ positions—as indexed on a pseudotetragonal cell with $a_{\text{guest}}^{\text{tetrag}}=a_{\text{host}}=7.00$ Å and $c_{\text{guest}}=2.05$ Å. This is illustrated in Fig. 2 for the four reflections around the calculated (021) position on this pseudotetragonal cell at (–0.2,2.2,1), (–0.2,1.8,1), (0.2,2.2,1), and (0.2,1.8,1). Figure 3 shows how these groups of guest reflections, lying in planes of diffuse scattering, relate to the host reflections. The guest reflections can be understood as coming from four domains of a primitive monoclinic structure (space-group $P2/m$) with $a_{\text{guest}}\sim b_{\text{guest}}=a_{\text{host}}/\sqrt{2}=5$ Å, $c_{\text{guest}}=2.05$ Å, and $\beta\sim93°$, and an atom on the 1a site at (0,0,0). Least-squares refinement of the positions of 14 reflections from the guest component gave lattice parameters of $a_{\text{guest}}=4.966(2)$ Å, $b_{\text{guest}}=4.951(7)$ Å, $c_{\text{guest}}=2.053(2)$ Å, and $\beta=94.7(1)°$ at 147 GPa. There are thus $16+2\times\frac{c_{\text{host}}}{c_{\text{guest}}}=19.3$ atoms in the host unit cell, and the volume per atom at 147 GPa is 8.62(3) Å^3.

The host and guest structures of tI19-Na at 147 GPa are shown in Fig. 4. The guest structures in tI19-Na, Rb-IV, and

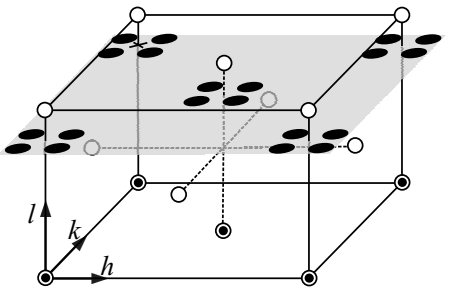

FIG. 3. Composite reciprocal lattice of tI19-Na showing host reflections (open spheres), and guest reflections broadened in the hk plane (filled circles) and lying in $(hk1)_{\text{guest}}$ plane of diffuse scattering. The $(hk0)$ reflections are from both components, as indicated. The cross (×) marks the $(021)_{\text{guest}}^{\text{tetrag}}$ position used in Fig. 2 and discussed in the text.

K-III are all different, being body-centered and C-face-centered tetragonal in Rb and K, respectively.[6,16] Monoclinic guest structures have been observed previously in Ba-IVa,[22] Sb-IV, and As-III,[23] and the monoclinic angle of 95° in Na is very similar to the 96° found in Ba-IVa.

In Rb-IV, it was possible to estimate the interchain correlation length from the additional width of the guest reflections.[21] By the same method, using the widths of two guest reflections [see Fig. 2(d)], we obtained a correlation length in Na at 147 GPa of 28(3) Å or about six times the interchain spacing of 4.95 Å at this pressure. This value is very similar to the correlation length of ~30 Å, or four times the interchain spacing, found previously in Rb-IV (Ref. 21) at 16.2 GPa, the lower pressure limit of its stability field. As noted, the guest reflections sharpen rapidly with pressure in Rb-IV, and the correlation length increases exponentially over just 0.6 GPa to reach more than 500 Å at 16.8 GPa. In contrast, the correlation length varies little with pressure in Na-tI19. The value of ~30 Å is obtained at 147 GPa, more than 20 GPa above the lower pressure limit of the phase, while the similar elongation of the guest reflections observed at 130 GPa suggests a correlation length not significantly different in terms of interchain spacings. It is not clear why the coherence length in Na should be so much less pressure

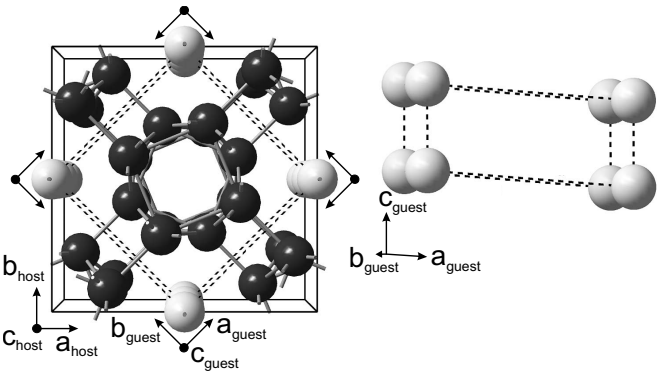

FIG. 4. The structure of tI19-Na shown in projection down the c axis with host atoms in dark gray and guest atoms in light gray. The guest-component unit cell is outlined with dashed lines, and a separate perspective view of the monoclinic guest structure on the same scale is shown.

dependent than in Rb. One possibility is that it is a result of the closeness of the melting curve to room temperature even at 150 GPa. However, studies of guest disorder in Rb-IV to 500 K showed no effect of temperature on the coherence length. Further studies on Na to higher pressures are required, in particular, to determine at what pressure the guest chains eventually order, if they do.

K, Rb, and Cs are known to exhibit abrupt reductions in optical reflectivity on transforming to their complex high-pressure phases,[24,25] accompanied by increased resistivity.[26] In Li, changes in reflectivity have been reported at pressures as low as 22 GPa,[27] and samples remain very dark up to the highest pressures studied.[12,27] The abrupt reduction in optical reflectivity in Na on transforming to the tI19 phase may also mark a transition to a higher resistivity phase, which persists to at least 155 GPa.

A determination of the electronic properties of tI19-Na, using either measurements of the resistivity or infrared reflectivity, represents a considerable experimental challenge. Moreover electronic structure calculations of tI19-Na are hampered by its incommensurate nature. While calculations of a commensurate approximant could, in principle, be conducted using a large supercell, it is not at all clear whether such calculations on a single approximant would capture the physics of the incommensurate system.

Therefore, we restrict our efforts here to a calculation of the electronic structure of the oP8 phase at 119 GPa immediately prior to the transition to tI19-Na. While not casting light on the properties of tI19-Na itself, these calculations demonstrate how much Na at Mbar pressures differs from the "simple metal" that it is at ambient conditions. The electronic structure calculations were performed with the full-potential augmented plane-wave WIEN2K code[28,29] using the experimental structural parameters of oP8-Na at 119 GPa, an $11\times17\times10$ mesh for k-point sampling (270 irreducible k points), and the generalized gradient approximation.[30] The electronic band structure of oP8-Na (Fig. 5) shows it to be a *semimetal* with an indirect $\Gamma-Y$ band overlap of ~0.7 eV and a low density of states (DOS) and a pseudogap near the Fermi level. The Fermi-surface pockets around Γ and Y contain only 0.0025 free electrons/atom and 0.0013 holes/atom, respectively, compared to 1 conduction electron/atom at ambient conditions. Consequently, the plasma frequencies are reduced to values of 2.7, 1.4, and 1.2 eV if the polarization is parallel to the crystallographic a, b, and c axes, respectively. The polarization anisotropy reflects the anisotropy of the electronic band structure.

The oP8-Na band structure shows that optical interband transitions can take place at energies from as low as 1 eV, i.e., throughout the visible range. This shifts the edge of metallic reflectivity to below 0.5 eV, i.e., into the infrared spectral range (not shown). For an oP8-Na sample in contact with a diamond anvil, the calculated reflectance is less than 10% at energies around 0.5 eV but rises toward higher energies due to the interband absorption, and it is at the ~50% level throughout the visible spectral range. For comparison, the calculated reflectance of a rhenium/diamond interface at ambient pressure is only ~20% while it is ~95% for a Na/diamond interface at ambient pressure (using the optical constants of Ref. 31).

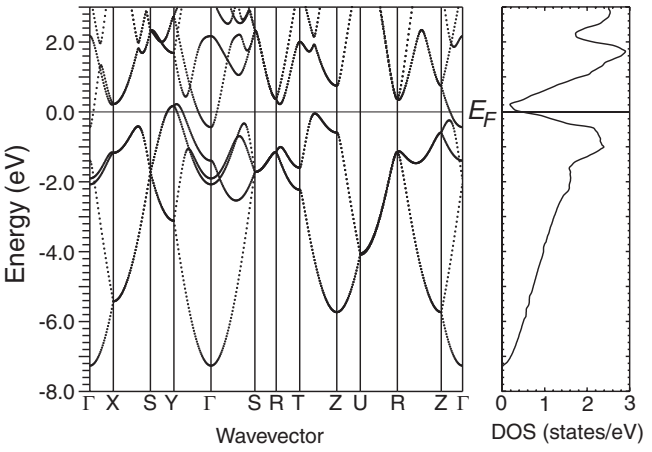

FIG. 5. Calculated electronic band structure and electronic DOS of oP8-Na at 119 GPa. E_F denotes the Fermi level.

What are the implications for tI19-Na? The abrupt darkening at the oP8-Na to tI19-Na transition is most likely due to changes in the interband excitations, i.e., a shift to higher energies and/or a reduction in oscillator strength. It is important to note that the observed darkening has little significance regarding the question whether tI19-Na is "less metallic" than oP8-Na because the ~50% reflectivity of the latter originates from the interband transitions rather than its free charge carriers. On the other hand, the fact that oP8-Na is already close to a metal-semiconductor transition makes it at least conceivable that the pseudogap could fully open at the transition and that Na-tI19 could be a semiconductor.

We thank W. Crichton and M. Mezouar for their help with the experiments. This work was supported by a research grant from the U.K. Engineering and Physical Sciences Research Council and facilities made available by the European Synchrotron Radiation Facility.

[1] N. W. Ashcroft and N. D. Mermin, *Solid State Physics* (Thomson Learning, London, 1976).

[2] N. W. Ashcroft, in *Condensed Matter at Higher Densities*, Proceedings of the International School of Physics "High Pressure Phenomena," edited by R. J. Hemley, G. L. Chiarotti, M. Bernasconi, and L. Ulivi (IOS, Amsterdam, 2002), p. 151.

[3] K. Syassen, in *Simple Metals at High Pressures*, Proceedings of the International School of Physics "High Pressure Phenomena" (IOS, Amsterdam, 2002), p. 266.

[4] M. Hanfland, K. Syassen, N. E. Christensen, and D. L. Novikov, Nature (London) **408**, 174 (2000).

[5] M. I. McMahon, R. J. Nelmes, and S. Rekhi, Phys. Rev. Lett.

87, 255502 (2001).
[6] M. I. McMahon, R. J. Nelmes, U. Schwarz, and K. Syassen, Phys. Rev. B **74**, 140102(R) (2006).
[7] K. Shimizu, H. Ishikawa, D. Takao, T. Yagi, and K. Amaya, Nature (London) **419**, 597 (2002).
[8] V. V. Struzhkin, M. I. Eremets, W. Gan, H. K. Mao, and R. J. Hemley, Science **298**, 1213 (2002).
[9] S. Deemyad and J. S. Schilling, Phys. Rev. Lett. **91**, 167001 (2003).
[10] E. Gregoryanz, O. Degtyareva, M. Somayazulu, R. J. Hemley, and H. K. Mao, Phys. Rev. Lett. **94**, 185502 (2005).
[11] E. Gregoryanz, L. F. Lundegaard, M. I. McMahon, C. Guillaume, R. J. Nelmes, and M. Mezouar, Science **320**, 1054 (2008).
[12] M. Hanfland, K. Syassen, N. E. Christensen, and D. L. Novikov, (unpublished).
[13] M. I. McMahon, E. Gregoryanz, L. F. Lundegaard, I. Loa, C. Guillaume, R. J. Nelmes, A. K. Kleppe, M. Amboage, H. Wilhelm, and A. P. Jephcoat, Proc. Natl. Acad. Sci. U.S.A. **104**, 17297 (2007).
[14] W. B. Pearson, *The Crystal Chemistry and Physics of Metals and Alloys* (Wiley-Interscience, New York, 1972).
[15] M. I. McMahon and R. J. Nelmes, Z. Kristallogr. **219**, 742 (2004).
[16] M. I. McMahon, S. Rekhi, and R. J. Nelmes, Phys. Rev. Lett. **87**, 055501 (2001).
[17] R. Boehler and K. De Hantsetters, High Press. Res. **24**, 391 (2004).
[18] M. Hanfland, K. Syassen, and J. Köhler, J. Appl. Phys. **91**, 4143 (2002).
[19] *SMART, SAINT, ASTRO and XPREP: Data Collection and Processing Software for the SMART System* (Bruker Analytical X-ray Systems, Inc., Madison, Wisconsin, 1995).
[20] *SHELXL-97: A Program for Single-Crystal-Structure Refinement*, edited by G. M. Sheldrick (University of Göttingen, Göttingen, 1997).
[21] M. I. McMahon and R. J. Nelmes, Phys. Rev. Lett. **93**, 055501 (2004).
[22] R. J. Nelmes, D. R. Allan, M. I. McMahon, and S. A. Belmonte, Phys. Rev. Lett. **83**, 4081 (1999).
[23] O. Degtyareva, M. I. McMahon, and R. J. Nelmes, Phys. Rev. B **70**, 184119 (2004).
[24] K. Takemura and K. Syassen, Phys. Rev. B **28**, 1193 (1983).
[25] K. Takemura and K. Syassen, Solid State Commun. **44**, 1161 (1982).
[26] A. Jayaraman, R. C. Newton, and J. M. McDonough, Phys. Rev. **159**, 527 (1967).
[27] A. F. Goncharov, V. V. Struzhkin, H. K. Mao, and R. J. Hemley, Phys. Rev. B **71**, 184114 (2005).
[28] P. Blaha, K. Schwarz, G. K. H. Madsen, D. Kvasnicka, and J. Luitz, in *WIEN2k, An Augmented Plane Wave+Local Orbitals Program for Calculating Crystal Properties*, edited by K. Schwarz (Techn. Universität Wien, Vienna, 2001).
[29] C. Ambrosch-Draxl and J. O. Sofo, Comput. Phys. Commun. **175**, 1 (2006).
[30] J. P. Perdew, K. Burke, and M. Ernzerhof, Phys. Rev. Lett. **77**, 3865 (1996).
[31] *CRC Handbook of Chemistry and Physics*, 85th ed., edited by D. R. Lide (CRC, Boca Raton, 2004).